A Lattice Boltzmann model for studying transient effects during imbibition-drainage cycles in unsaturated soils

S.A. Galindo-Torres[a,b], A. Scheuermann[a], L. Li[b], D. M. Pedroso[a], D. J. Williams[a]

[a] *Geotechnical Engineering Centre. School of Civil Engineering, The University of Queensland, Brisbane QLD 4072, Australia*

[b] *National Centre for Groundwater Research & Training. School of Civil Engineering, The University of Queensland, Brisbane QLD 4072, Australia*

Abstract

This paper presents a numerical model based on the Lattice Boltzmann Method (LBM), developed for studying dynamic responses of an unsaturated porous medium to periodic imbibition and drainage induced by a cyclic water table movement. The model includes gravity which helps defining an hydraulic head. The model predicted an incremental increase of the overall water content in the medium over each cycle prior to a quasi-steady oscillatory state, a *hydraulic ratcheting effect* that has been previously observed in laboratory experiments. An empirical model was proposed to combine the transient and harmonic variations of the volumetric water content. The parameters of this empirical model were examined against physical quantities including the frequency of the driving water table oscillations and the porosity of the porous medium. The findings presented here may help to improve the formulation of constitutive models that are able to describe hydraulic processes of unsaturated soils.

Keywords: Lattice Boltzmann Methods, Unsaturated soil physics

1. Introduction

Infiltration and drainage in unsaturated soils are important processes related to variations in boundary conditions at the interfaces with the atmosphere, surface and groundwater bodies caused by, for example, evaporation-condensation, tidal oscillations and rainfall. These processes produce so-called dynamic effects [1] on the water retention capabilities of the soil. These effects have been studied extensively with models proposed to take into account the deviation from equilibrium conditions as a perturbation (the so-called τ model [2, 3]). However, the accuracy of these models tends to deteriorate when the capillary pressure varies faster than a soil specific critical rate [3].

A numerical model is developed to simulate transient flow processes of pore water in an unsaturated soil column subjected to periodic forcing conditions, using a multiphase

Email address: s.galindotorres@uq.edu.au (S.A. Galindo-Torres)

multicomponent (MP-MC) implementation of the LBM. Water evolution in unsaturated soils is usually described by Richard's equation [4], which considers water retention curves at equilibrium. In contrast, the LBM solves the Boltzmann equation, which is a more general and fundamental description of the fluid dynamics [5]. The application of the Boltzmann equation is not only for multiphase-multicomponent fluid dynamics [6, 7, 8]; it encompasses a broader range of conditions including laminar and turbulent flow in the pore space [9, 10], interactions with solid boundaries formed by grains of complex shapes [11] and moving solid particles modelled using the Discrete Element Method [12]. Also, it has shown potential to describe key quantities at the pore scale such as the fluid distribution inside the pore network [13].

The LBM scheme has shown enough power to solve different partial differential equations, unrelated to porous media flow problems, adding more versatility to its modelling capabilities. Among these applications the simulation of relativistic fluids [14, 15], the solution of Maxwell equations [16, 17] and the study of classical wave propagation problems [18] can be mentioned. The level of detail of a LBM simulation allows the observation of microscopic phenomena with ease. However, the increase of the level of detail is computational expensive.

LBM has previously been used to reproduce the water retention curve of porous media in equilibrium conditions [19, 20]. However, there have been no studies reported using LBM to explore dynamic effects on imbibition-drainage processes in porous media. In the present study, these processes were simulated in a modelled soil column subjected to a harmonic hydraulic head fluctuation. These simulations are aimed to examine particularly the transient component of the water saturation response to the periodic head fluctuation. In particular, when the cycles take place faster than a characteristic equilibrium time, there is an incremental saturation increase after each cycle as reported in the literature [21]. This phenomenon, herein referred to as *hydraulic ratcheting*, is the subject of the detailed study in this paper.

The rest of the paper is structured as follows: In Sec. 2, the implementation of the LBM model used in this study is briefly described. In Sec. 4, the transient response of simulated water saturation is examined in detail with an empirical model proposed for describing the saturation evolution. Finally, in Sec. 5, discussions and implications of the finding from the current work are presented.

2. Model

The LBM D2Q9 scheme [22] was adopted. Within this scheme, the space is divided into a square grid. To solve the Boltzmann equation, further discretization is needed in the velocity domain. A set of nine discrete velocities (Fig. 1), each with an associated probability function f_i, were assigned to every cell. The discrete velocities are defined as follows:

$$\begin{aligned} \vec{\boldsymbol{e}}_0 &= (0,0), \\ \vec{\boldsymbol{e}}_{i=1,2,3,4} &= C\left(\cos(\pi(i-1)/2), \sin(\pi(i-1)/2)\right), \\ \vec{\boldsymbol{e}}_{i=5,6,7,8} &= C\sqrt{2}\left(\cos(\pi(i-7/2)/2), \sin(\pi(i-7/2)/2)\right), \end{aligned} \tag{1}$$

where C is a lattice constant, $= \delta_x/\delta_t$ with δ_t being the time step and δ_x the side of each square cell. To define the fluid velocity $\vec{\boldsymbol{u}}$ and density ρ at a given cell, the following relations were applied:

$$\begin{array}{ll} \rho = & \sum_{i=0}^{8} f_i \\ \rho\vec{\boldsymbol{u}} = & \sum_{i=0}^{8} f_i \vec{\boldsymbol{e}}_i \end{array} \tag{2}$$

It is also important to assign a set of weights ω_i for the velocities. For the D2Q9 scheme, such weights are:

$$\begin{array}{ll} \omega_0 = & \frac{4}{9}, \\ \omega_{i=1,2,3,4} = & \frac{1}{9}, \\ \omega_{i=5,6,7,8} = & \frac{1}{36}, \end{array} \tag{3}$$

After defining the velocities, an evolution rule is implemented to solve the Boltzmman equation [9]:

$$f_i(\vec{\boldsymbol{x}} + \delta_t\vec{\boldsymbol{e}}_i, t + \delta_t) = f_i(\vec{\boldsymbol{x}}, t) + \Omega_{col}, \tag{4}$$

where $\vec{\boldsymbol{x}}$ is the position of the given cell, t is the current time and Ω_{col} is an operator for the collision of all the particles that exist inside the cell. For this study, the widely accepted Bhatnagar Gross Krook (BGK) model for the collision operator [23] was used, which assumes that the collision processes drive the system into an equilibrium state given by an equilibrium function f_i^{eq},

$$\Omega_{col} = \frac{f_i^{eq} - f_i}{\tau} \tag{5}$$

with τ being a characteristic relaxation time. It has been demonstrated that the Navier Stokes equations for fluid flow [5] are recovered if,

$$f_i^{eq} = \omega_i\rho\left(1 + 3\frac{\vec{\boldsymbol{e}}_i \cdot \vec{\boldsymbol{u}}}{C^2} + \frac{9(\vec{\boldsymbol{e}}_i \cdot \vec{\boldsymbol{u}})^2}{2C^4} - \frac{3u^2}{2C^2}\right) \tag{6}$$

and the dynamic viscosity of the fluid ν is given by,

$$\nu = (\tau - 0.5)\frac{\delta_x^2}{3\delta_t}. \tag{7}$$

Eq. 7 imposes a constraint on τ, which must be greater than 0.5 for the viscosity to be physically correct. It is also known that values close to 0.5 produce unstable numerical behaviour [9]; hence it is advisable to keep its value close to one.

In order to model multicomponent and multiphase flows as well as body forces such as the gravity force [24], a net force is introduced for each cell. The net force $\vec{\boldsymbol{F}}$ modifies the velocity used in the calculation of the equilibrium function as follows,

$$\vec{\boldsymbol{u}}' = \vec{\boldsymbol{u}} + \frac{\delta_t\vec{\boldsymbol{F}}}{\rho}. \tag{8}$$

In the case of gravity, the force is simply $\vec{\boldsymbol{F}}_g = \rho\vec{\boldsymbol{g}}$ where $\vec{\boldsymbol{g}}$ is the gravitational acceleration [25]. In the present study gravity has been included allowing a phreatic limit to be defined which will prove useful for the simulation analysis later on.

Multiphase flows are modelled in LBM by introducing attractive forces $\vec{\boldsymbol{F}}_a$ representing the interaction between the fluid molecules. In this paper, the Shan-Chen model [26] was used. With this scheme, the attractive forces are given by:

$$\vec{\boldsymbol{F}}_a = -G_a \psi(\vec{\boldsymbol{x}}) \sum_{i=1}^{8} \omega_i \psi(\vec{\boldsymbol{x}} + \delta_t \vec{\boldsymbol{e}}_i) \vec{\boldsymbol{e}}_i, \tag{9}$$

where G_a is a constant representing the intensity of the attraction and the function ψ is an interaction potential which should be bounded and increasing monotonically with density. For this study, the following form was taken [9]:

$$\psi = \psi_0 \exp\left(-\rho_0/\rho\right), \tag{10}$$

with ψ_0 and ρ_0 being constant.

It is known that for this model the fluid follows the following equation of state (EOS) for the fluid pressure p [9]:

$$p = \frac{C^2}{3}\rho + \frac{G_a}{6} C^2 \psi^2(\rho). \tag{11}$$

Unfortunately, this model suffers a critical drawback: The liquid phase may be highly compressible. Solutions have been proposed to address this issue. For example, rearranging Eq. 11 for $\psi(\rho)$ yields [19]:

$$\psi(\rho) = \sqrt{\frac{6p - 2C^2\rho}{G_a C^2}}. \tag{12}$$

Any possible EOS can be simulated by assigning its functional form to p in Eq. 12, in particular EOSs with low compressibility where $\frac{\partial p}{\partial \rho} \to \infty$ for a given density. Since G_a is negative, in the case of attractive forces, $6p - 2C^2\rho < 0$ must hold for $\psi(\rho)$ to remain in the real domain and physically meaningful. In other words, the pressure given by a non ideal EOS should be smaller than the pressure given by the ideal EOS for the same density. For realistic simulations this criterion is not often met. As an example, a Van der Waals EOS will eventually be higher than the ideal counterpart because of the singularity term and hence the ψ function will be imaginary. Consequently Eq. 10 was used instead for this study. The ultimate solution for this problem is the introduction of the hard sphere repulsion to the LBM formalism. However, this is not easy and has not yet been done to the best of our knowledge.

With Eqs. 10 and 11 applied for large densities, the pressure follows a shifted ideal gas law. The simulated fluid compressibility can be estimated based on the inverse of the following derivative,

$$\frac{\partial p}{\partial \rho} = \frac{C^2}{3}. \tag{13}$$

It is clear that the simulated fluid compressibility is controlled by the lattice speed parameter C. With large values of C, $\frac{\partial p}{\partial \rho}$ can be kept large to approximate an incompressible fluid. However changing C changes also other parameters, such as the surface tension, and therefore is a solution that has to be used with care specially for multiphase simulations. Therefore it

is important to check the effect of the compressibility (for instance with the Mach number) on the obtained results.

More than one component can be simulated by assigning an independent lattice to each of them [27]. Then different fluids (lattices) interact through repulsive forces $\vec{\boldsymbol{F}}_r$ in a similar way to that of Eq. 9. For example, the interaction of component 1 (indicated by subscript 1) with component 2 (subscript 2) can be expressed as follows,

$$\vec{\boldsymbol{F}}_r = -G_r \rho_1(\vec{\boldsymbol{x}}) \sum_{i=1}^{8} \omega_i \rho_2(\vec{\boldsymbol{x}} + \delta_t \vec{\boldsymbol{e}}_i) \vec{\boldsymbol{e}}_i, \tag{14}$$

where G_r controls the repulsion intensity – its value is always positive – and the potential (ψ) terms have been replaced by the densities of the two components/phases.

With multiple components included, the equilibrium velocity (Eq. 2) must be corrected, i.e.,

$$\vec{\boldsymbol{u}} = \frac{\sum_\sigma \sum_{i=1}^{8} \frac{1}{\tau_\sigma} f_i^\sigma \vec{\boldsymbol{e}}_i}{\sum_\sigma \frac{\rho_\sigma}{\tau_\sigma}} \tag{15}$$

where the contribution of each component σ has been accounted for [27].

Finally, the interaction of the fluids with solids is two-fold. Firstly, the fluid must be repelled by solid cells upon collision. Hence, the bounce-back boundary condition [9] was implemented for cells that are tagged as solids: after the collision step, the distribution functions are swapped symmetrically, i.e.,

$$f_{-i} = f_i \tag{16}$$

where the subscript $-i$ refers to the opposite direction to the i-th velocity. Secondly, to model the capillary effect the fluid should also be attracted to the solid in a similar way to that expressed by Eq. 9,

$$\vec{\boldsymbol{F}}_a = -G_s \psi(\vec{\boldsymbol{x}}) \sum_{i=1}^{8} \omega_i s(\vec{\boldsymbol{x}} + \delta_t \vec{\boldsymbol{e}}_i) \vec{\boldsymbol{e}}_i, \tag{17}$$

where G_s controls the intensity of the fluid-solid attraction and s is a logical constant, = 1 if the cell has at least one neighbouring cell tagged as solid and 0 otherwise. As will be shown, values of parameters G_a, G_r and G_s can be set accordingly to simulate required fluid properties including contact angle of interface, surface tension and immiscibility of multiple components.

3. Simulation setup

It is commonly the case that LBM models are based on lattice units. In such units, $\delta_t = \delta_x = C = 1$. The lattice units, however, can be converted to physical ones based on dimensional analysis to enable comparison of the simulation results with experimental data and analytical solutions. The LBM approach has been successfully validated in a broad range of

applications [9]. In this work, lattice units are used as well. The multicomponent-multiphase scheme described above was implemented to model two immiscible fluids, representing air and water, respectively. To achieve this, the attraction constants G_a were set to different values for the two fluids. The corresponding values for the parameters adopted for the work are listed in Table 1. The three LBM parameters described above (G_a,G_r and G_s) control measurable quantities such as the liquid and vapour densities for each component, the surface tension and the contact angle with solid surfaces. Fig. 2 shows results of a contact angle simulation based on the values for the LBM parameters given in table 1.

The first fluid has a non-zero G_a, only under which Eq. 11 applies. The parameter value used ensured a liquid phase density at zero pressure of $\rho_l = 1119.2 m_u/\delta_x^2$ (m_u equal to mass units which is equivalent to a unit density multiplied by the area of the LBM cell δ_x^2) obtained by solving 11 for the third root value over the spinodal point. Greater pressures would compress the fluid and increase its density.

For problems involving multi-component fluids, the surface tension at the interface is a critical quantity for setting the simulated condition; and thus it is useful to determine this quantity based on the LBM parameter values used in the simulations and convert it from the lattice units system to the physical system. For that purpose, a set of bubble simulations were carried out. Bubbles of different radii made of the light fluid (gas) were placed into a domain filled with the denser one (water). Simulation results in snapshots are shown in Fig. 3. To measure the surface tension σ, the Young-Laplace equation was used,

$$P_{in} - P_{out} = \frac{\sigma}{R}, \tag{18}$$

where P_{in} and P_{out} are the pressure of the mixed fluid inside and outside the bubble, respectively; and R is the bubble's radius. To measure the pressure p at a given point, Eq 11 was used for each component with an extra (third) term added to account for the mixing [20], i.e.,

$$p = \left(\sum_{i=1}^{2} \frac{C^2}{3} \rho_i + \frac{G_a^i}{6} C^2 \psi^2(\rho_i) \right) + G_r C^2 \rho_1 \rho_2. \tag{19}$$

The capillary pressure $P_c = P_{in} - P_{out}$ is shown as a function of the inverse of the bubble's radius in Fig. 4. The slope of the line gives the surface tension ($94.5 \pm 1.3 m_u \delta_t^{-2}$).

The set-up for the simulations for the investigation of the dynamic response is schematically shown in Fig. 5. The granular medium was generated by filling the model domain with a poly-disperse random array of solid disks until the desired porosity was obtained. The left and right boundaries were all composed of solid cells, i.e., no-flow boundaries (impermeable) for both fluids. The top boundary was also tagged as solid for the first fluid (water). At the bottom boundary, the density ρ_b was set to vary in time to simulate oscillations of the water pressure. In contrast, for the second fluid (gas) the bottom boundary was set to be impermeable while a constant pressure (density) was imposed at the top boundary allowing both gas in- and out-flow[28].

It is expected that by setting a density value at the bottom boundary, the system will relax eventually until the pressure at the bottom equals the pressure of the fluid column

under gravity. Hence, simulations were carried out without disks to find the dependence between the imposed bottom density ρ_b and the maximum height h reached by the fluid at equilibrium. As an example, the evolution of the fluid column from a simulation is shown in Fig. 6.

In Fig. 7, the maximum fluid height varying with a set of ρ_b values is shown. It can be observed that a linear dependence of $H = A\rho_b + B$ (with $A = 0.056$ and $B = 1.337$) provides a good fit. It is useful to refer to this height as the hydraulic head for the chosen g value. In theory, the hydraulic head H should follow,

$$H = \frac{p(\rho_b)}{\bar{\rho} g}, \tag{20}$$

where $\bar{\rho}$ is the mean density and $p(\rho)$ is given by Eq. 11. However, comparison between the H values calculated by this equation and those presented in Fig. 7 shows a noticeable discrepancy. This indicates that Eq. 11 is not suitable for finding the fluid pressure at the cell level for this problem with gravity involved and no correction has been made to the best of our knowledge. However, the importance of this discrepancy is not critical since an empirical relation between the equilibrium height and the imposed density at the bottom has been found. Therefore, the simulation results of the water saturation are analysed in relation to the height H (representing the hydraulic head as circles in Fig. 7) instead of the density imposed at the bottom boundary ρ_b. To the best of our knowledge this is the first time a phreatic surface in the presence of gravity is properly defined in an LBM soil column simulation.

4. Transient response to imposed harmonic head fluctuations

The purpose of the simulations was to study the transient response of the modelled soil column to harmonic hydraulic head fluctuations imposed at the domain bottom boundary, i.e.,

$$h(t) = 0.5h_0(1 - \cos(\omega t)). \tag{21}$$

with h_0 being a constant that controls the average water saturation. Should the water be able to invade the void spaces without any resistance, there would be an immediate response of the saturation Sr to the imposed head fluctuation $h(t)$. However, due to the hydraulic conductivity of the sample, as a measure for the resistance of the porous medium to the water flow, there is a lag between the two signals as observed experimentally [29].

To explore this phenomenon with the LBM set-up, two dynamic situations with 16 and 6 cycles for a given timespan were simulated and compared with the equilibrium condition. As can be seen in Fig. 8, due to the transient nature of the simulation with the highest frequency (16 cycles), an incremental increase of the water saturation was evident after each cycle until a quasi-steady state (equilibrium) was reached. For the lower frequency (6 cycles), the transient component became bounded and disappeared for the equilibrium simulation as expected. Fig. 9 shows the saturation evolution over time for different frequencies of the driving head fluctuations. Two different behaviours can be observed: a harmonic response

with the same frequency as that of $h(t)$, and additionally a growing trend with a clear limit, which is likely to be well captured by an exponential function with an asymptotic value of Sr_{max}. The asymptotic value appeared to be independent of the frequency of the driving head fluctuation. This exponential increase trend was more noticeable for large frequencies, where the amplitude of the harmonic component was small. A superposition of these two behaviours/effects may be proposed as follows,

$$Sr(t) = A(\omega)\cos(\omega t + \phi) + Sr_{max}\left(1 - \exp(-t/t_c)\right), \tag{22}$$

where A is the amplitude of the harmonic Sr oscillations, ϕ is a phase difference between Sr and h produced by the hydraulic lag, and t_c is a characteristic time for the exponential transient function.

To explore the validity of Eq. 22, a Fourier analysis was conducted to separate the harmonic and exponential components. In Fig. 10, the discrete Fourier transformation amplitudes are shown for each frequency. The anomalous peak represents the frequency of the imposed hydraulic head. This peak was filtered out by interpolation of the surrounding points. The inverse Fourier transformation was then applied to the filtered spectrum. Fig. 11 shows the water saturation variation with time after the harmonic signal had been filtered by the Fourier method. With the same filtering method applied to all the simulations (with 16 different frequencies as shown in Fig. 9), the average fitting parameters for the exponential function were found to be $Sr_{max} = 0.58 \pm 0.02$ and $t_c\sqrt{g/H} = 12.67 \pm 0.05$. The errors associated with the fitting were small for these values; thus it may be concluded that both parameters do not depend on ω.

Although Sr_{max} and t_c do not depend on ω, it is expected that the amplitude of the harmonic component (A) and its phase difference (ϕ) are functions of the frequency. Indeed Fig. 12 shows the amplitude variations with frequency. Previous studies have found a power law dependence of A on ω for large frequencies, which seemed to be also evident in the present simulations [29, 30]. The phase ϕ was negative, as given by the lagged signal. For small values of ω, ϕ approached zero and the oscillation of Sr became synchronised with the driving head fluctuation.

At this point it is important to check if the observed lag has a strong dependence on the compressibility of the LBM fluid. To check this, the average Mach number is measured for the initial cycle, which is the one with the fastest change in water saturation. The average velocity is calculated spatially over all the cells containing the wetting fluid and temporally over the full cycle. The obtained Mach number for the first cycle of the highest frequency (18 cycles over the total time of $4.0 \times 10^5\ \delta_t$) is 0.029 which is below the level (Mach number ~ 0.1) where compressibility effects should be considered. Later cycles, and cycles for lower frequencies will have Mach numbers below this level as well. Therefore, although the observed lag should have a contribution due to the compressibility of the fluid, it is largely dependent on the porous medium and the capillary action in this study.

The soil structure would also play an important role in the development of the transient condition, mainly due to its influence on hydraulic conductivity. Further simulations were conducted with varying porosity. The results plotted in Fig. 13 show the dependence of t_c on

the porosity. As expected, t_c decreased with increasing porosity as a result of the increased hydraulic conductivity giving a more responsive soil system. Porosity is affected by internal stresses, which may lead to large variations of hydraulic conductivity with depth, especially when denser portions of the soil are encountered. It is thus expected that the *hydraulic ratcheting* effect, examined here and observed experimentally [29], may be more pronounced in deep soil layers.

5. Discussions and concluding remarks

In this paper, a numerical model using the Shan-Chen LBM formulation [26] has been developed for studies of the behaviour of multiphase and multicomponent fluids in soils. The study includes the effect of gravity, rarely considered in LBM simulations of multiphase fluids. Thanks to this, a water table can be defined and it has been shown that its height (the hydraulic head) can be controlled with the density boundary condition imposed at the domain's bottom.

By imposing a cyclic water table, important transient effects have been observed. In particular, the *hydraulic ratcheting* phenomenon, characterised by a gradual accumulation of volumetric water content was investigated through simulations based on this model. Based on the analysis of the simulation results, it can be concluded that the saturation Sr evolves according to Eq. 22 which is similar to empirical equations found during soil column experiments [29]. This relationship depends on four independent parameters: the amplitude A and the phase difference (lag) ϕ of the harmonic component, and a transient component defined by an equilibrium saturation Sr_{max} and a relaxation time t_c. It was found that the frequency ω of the imposed head fluctuation affects strongly the parameters A and ϕ, but it does not influence the transient component.

Porosity affects the characteristic time t_c: as expected for a large porosity, t_c decreases, reducing the timespan needed to reach the equilibrium condition. The parameter t_c is independent of the driving head fluctuation and may be considered as an intrinsic parameter of the soil. It may be further hypothesised that this characteristic time also depends on the soil particle size distribution, shape, and packing pattern. Therefore, t_c is likely to be linked to the soil hydraulic conductivity.

The relationship expressed by Eq. 22 is an analogue to the RC (Resistance-Capacitance) circuit. In the latter, a complex impedance produces a lag between the input signal V_{in} and the voltage at the capacitor V_C. The analytical solution of the capacitor voltage for an input voltage of the form $V_{in} = V_0(1 - \cos(\omega(t))/2$ is:

$$V_C = A(\omega)\cos(\omega + \phi) + \frac{V_0}{2}\left(1 - \exp(-t/t_c)\right) \tag{23}$$

where $A = 0.5V_0/\sqrt{(\omega t_c)^2 + 1}$, $\phi = \arctan(\omega t_c)$ and $t_c = RC$ (the product of the resistance R and the capacitance C). According to the analogy, R for the soil would be proportional to the inverse of the hydraulic conductivity; and the capacitance must be related to the porosity, since it would be an indication of how much water the system can store. The lag characterised by t_c and ϕ produced by the complex impedance is consistent with the

complex porosity used in the literature [29, 30] to study the phase difference between the driving and responding hydraulic heads. Despite the similarity between Eqs. 22 and 23, the functional forms for the parameters in Eq. 22 (A, t_c and ϕ) unfortunately cannot be derived from the analogy.

In summary, the *hydraulic ratcheting* phenomenon examined here has important implications for studies of shallow groundwater systems, especially those subjected to cyclic wetting and drying processes associated with boundary condition changes (e.g., evaporation-condensation and tide-induced oscillations). The transient effect revealed represents a considerable variation of water storage in the unsaturated soil and may influence water balance in the subsurface environment over large scales. Although local-scale soil water retention characteristics were not investigated in this study, it is possible that the transient effect shown in the soil column is related to dynamic capillary pressure, which is not incorporated in commonly used soil water retention models using the equilibrium assumption. The presented LBM implementation can be extended to 3D and used to study more complex variations of the water table.

[1] S. Hassanizadeh, M. Celia, H. Dahle, Dynamic effect in the capillary pressure–saturation relationship and its impacts on unsaturated flow, Vadose Zone Journal 1 (1) (2002) 38–57.

[2] V. Joekar-Niasar, S. Hassanizadeh, H. Dahle, Non-equilibrium effects in capillarity and interfacial area in two-phase flow: dynamic pore-network modelling, Journal of Fluid Mechanics 655 (1) (2010) 38–71.

[3] G. Goel, D. O'Carroll, Experimental investigation of nonequilibrium capillarity effects: Fluid viscosity effects, Water Resources Research 47 (9) (2011) W09507.

[4] M. Kirkland, R. Hills, P. Wierenga, Algorithms for solving Richards' equation for variably saturated soils, Water resources research 28 (8) (1992) 2049–2058.

[5] X. He, L. Luo, Lattice boltzmann model for the incompressible navier–stokes equation, Journal of Statistical Physics 88 (3) (1997) 927–944.

[6] K. Kono, T. Ishizuka, H. Tsuda, A. Kurosawa, Application of lattice boltzmann model to multiphase flows with phase transition, Computer Physics Communications 129 (13) (2000) 110 – 120. doi:10.1016/S0010-4655(00)00098-9.
URL `http://www.sciencedirect.com/science/article/pii/S0010465500000989`

[7] N. Takada, M. Misawa, A. Tomiyama, S. Fujiwara, Numerical simulation of two- and three-dimensional two-phase fluid motion by lattice boltzmann method, Computer Physics Communications 129 (13) (2000) 233 – 246. doi:10.1016/S0010-4655(00)00110-7.
URL `http://www.sciencedirect.com/science/article/pii/S0010465500001107`

[8] T. Ramstad, P. ? ren, S. Bakke, Simulation of two-phase flow in reservoir rocks using a lattice boltzmann method, SPE Journal 15 (4) (2010) 917–927.

[9] M. Sukop, D. Thorne, Lattice Boltzmann modeling: An introduction for geoscientists and engineers, Springer Verlag, 2006.

[10] M. Schaap, I. Lebron, An evaluation of permeability of statistically reconstructed three-dimensional pore structures with lattice boltzmann simulations, Developments in Water Science 55 (2004) 15–22.

[11] C. Pan, L. Luo, C. Miller, An evaluation of lattice boltzmann schemes for porous medium flow simulation, Computers & fluids 35 (8-9) (2006) 898–909.

[12] Y. Feng, K. Han, D. Owen, Combined three-dimensional lattice boltzmann method and discrete element method for modelling fluid–particle interactions with experimental assessment, International Journal for Numerical Methods in Engineering 81 (2) (2010) 229–245.

[13] M. Sukop, H. Huang, C. Lin, M. Deo, K. Oh, J. Miller, Distribution of multiphase fluids in porous media: Comparison between lattice boltzmann modeling and micro-x-ray tomography, Physical Review E 77 (2) (2008) 026710.

[14] M. Mendoza, B. Boghosian, H. Herrmann, S. Succi, Fast lattice boltzmann solver for relativistic hydrodynamics, Physical review letters 105 (1) (2010) 14502.
[15] P. Romatschke, Relativistic (lattice) boltzmann equation with nonideal equation of state, Physical Review D 85 (6) (2012) 065012.
[16] P. Dellar, Electromagnetic waves in lattice boltzmann magnetohydrodynamics, EPL (Europhysics Letters) 90 (5) (2010) 50002.
[17] M. Mendoza, J. Munoz, Three-dimensional lattice boltzmann model for electrodynamics, Physical Review E 82 (5) (2010) 056708.
[18] H. Lai, C. Ma, Lattice boltzmann model for generalized nonlinear wave equations, Physical Review E 84 (4) (2011) 046708.
[19] H. Huang, Z. Li, S. Liu, X. Lu, Shan-and-chen-type multiphase lattice boltzmann study of viscous coupling effects for two-phase flow in porous media, International Journal for Numerical Methods in Fluids 61 (3) (2009) 341–354.
[20] M. Schaap, M. Porter, B. Christensen, D. Wildenschild, Comparison of pressure-saturation characteristics derived from computed tomography and lattice boltzmann simulations, Water Resour. Res 43 (12) (2007) W12S06.
[21] A. Scheuermann, Water content dynamics in unsaturated soils - results of experimental investigations in laboratory and in situ, Unsaturated Soils: Advances in Geo-engineering : Proceedings of the 1st European Conference on Unsaturated Soils (2008) 197–203.
[22] P. Gresho, R. Sani, On pressure boundary conditions for the incompressible navier-stokes equations, International Journal for Numerical Methods in Fluids 7 (10) (1987) 1111–1145.
[23] Y. Qian, D. d'Humieres, P. Lallemand, Lattice bgk models for navier-stokes equation, EPL (Europhysics Letters) 17 (1992) 479.
[24] N. S. Martys, H. Chen, Simulation of multicomponent fluids in complex three-dimensional geometries by the lattice boltzmann method, Phys. Rev. E 53 (1996) 743–750. doi:10.1103/PhysRevE.53.743.
URL http://link.aps.org/doi/10.1103/PhysRevE.53.743
[25] J. Buick, C. Greated, Gravity in a lattice boltzmann model, Physical Review E 61 (5) (2000) 5307.
[26] X. Shan, H. Chen, Lattice boltzmann model for simulating flows with multiple phases and components, Phys. Rev. E 47 (1993) 1815–1819. doi:10.1103/PhysRevE.47.1815.
URL http://link.aps.org/doi/10.1103/PhysRevE.47.1815
[27] X. Shan, G. Doolen, Multicomponent lattice-boltzmann model with interparticle interaction, Journal of Statistical Physics 81 (1) (1995) 379–393.
[28] Q. Zou, X. He, On pressure and velocity flow boundary conditions and bounceback for the lattice boltzmann bgk model, Arxiv preprint comp-gas/9611001.
[29] N. Cartwright, P. Nielsen, P. Perrochet, Influence of capillarity on a simple harmonic oscillating water table: Sand column experiments and modeling, Water resources research 41 (8) (2005) W08416.
[30] N. Cartwright, P. Nielsen, L. Li, Experimental observations of watertable waves in an unconfined aquifer with a sloping boundary, Advances in water resources 27 (10) (2004) 991–1004.

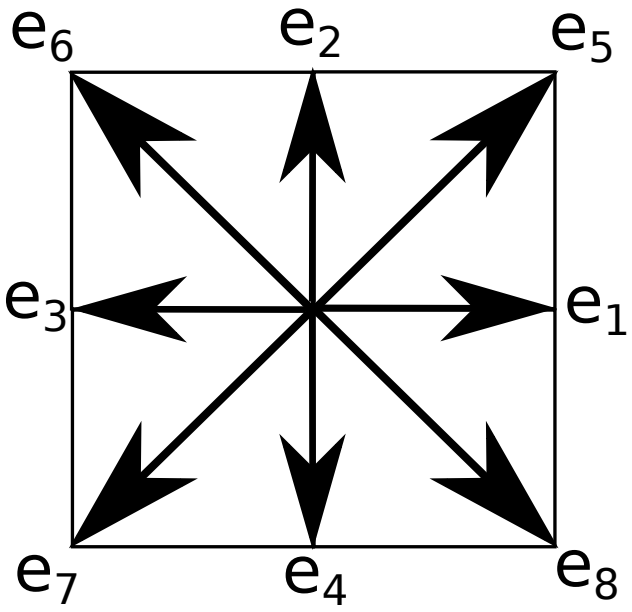

Figure 1: In the D2Q9 scheme, the domain is divided into a square grid with each cell simulated through 9 discrete velocities ($\vec{e}_i$), each associated with a distribution function f_i.

Table 1: Parameters values used in the simulations. The superscript 1 is used for the denser fluid representing water. The values of ψ_0 and ρ_0 are the same for both fluids

Parameter	Value
G_a^1	-200.0
G_a^2	0.0
ψ_0	4.0
ρ_0	200
G_r	0.001
g	0.001
τ	1.0
Final time	4.0×10^5 δ_t
Domain width	400 cells
Domain height	600 cells

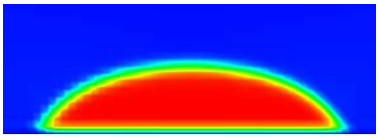

Figure 2: Liquid bubble at the equilibrium with $G_s^1 = -600.0$ ensuring a contact angle of 31°.

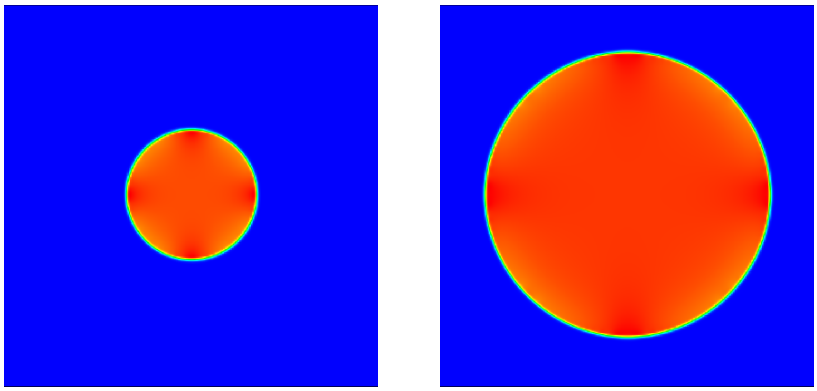

(a) (b)

Figure 3: Bubble simulations of a lighter fluid (red) inside the denser one (blue) for two different radii: a) 20 δ_x and b) 70 δ_x

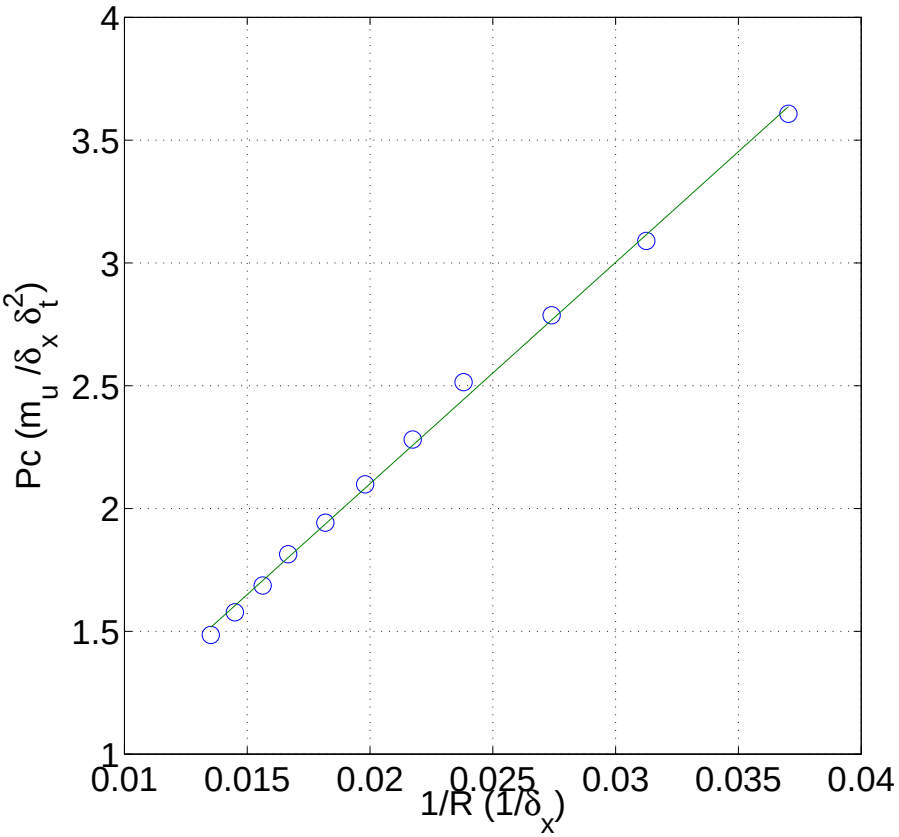

Figure 4: Capillary pressure P_c as a function of bubble radius. The slope of the line determines the surface tension between the fluids ($94.5 \pm 1.3 m_u \delta_t^{-2}$).

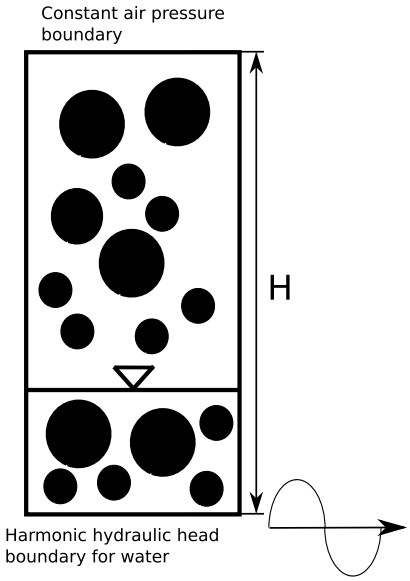

Figure 5: Simulation set-up. The no-flow boundary cells of the LBM domain were tagged as solid. The bounce back rule of Eq. 16 were applied to them but with cohesion (Eq. 17) turned off to mitigate the effects of the boundaries. The water table oscillated with time during the simulation due to the varying pressure head imposed at the bottom boundary.

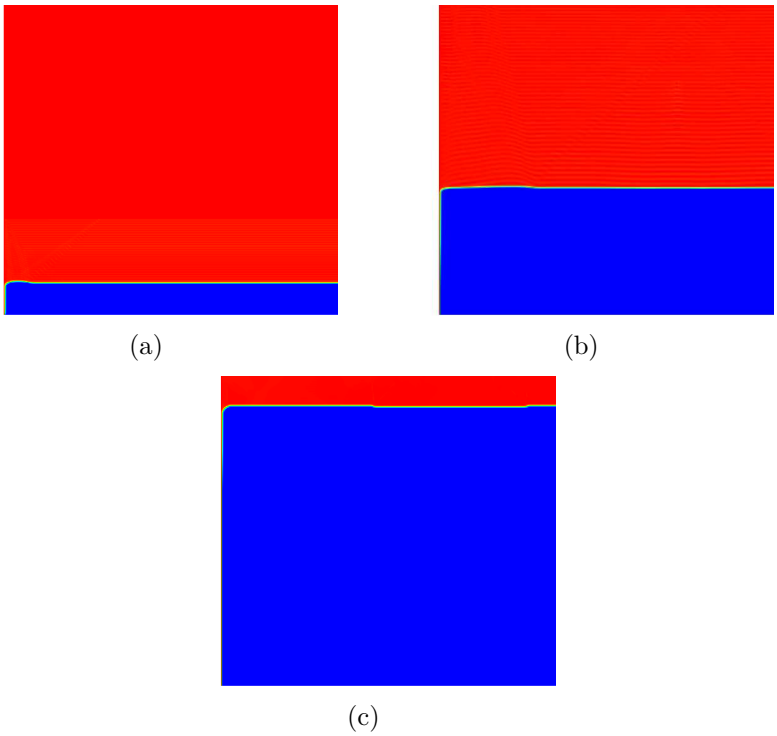

Figure 6: Evolution of the fluid column from a simulation in which the bottom density was fixed with a constant value and an equilibrium condition was reached at the end.

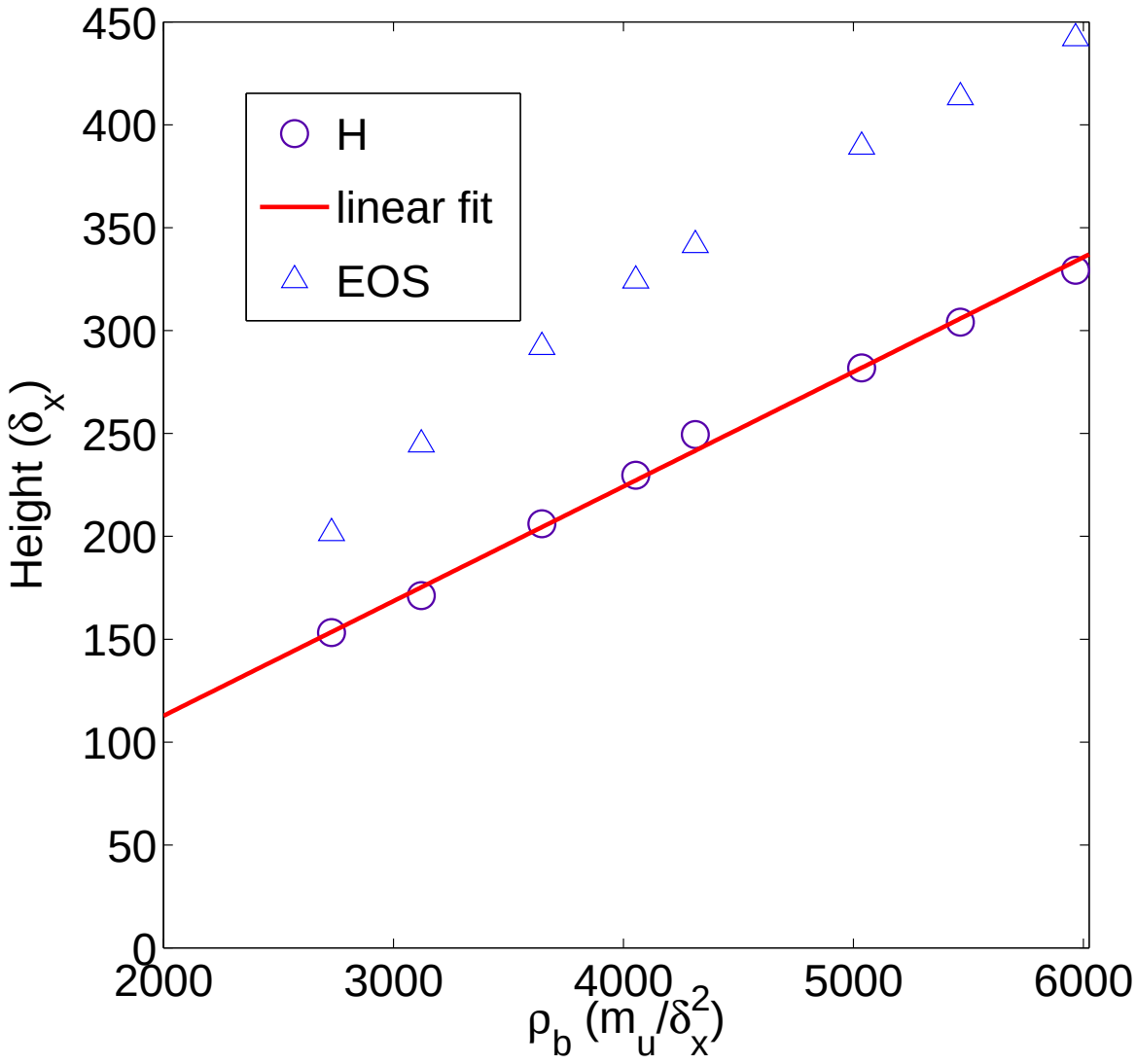

Figure 7: Maximum fluid height H varying with density (pressure) imposed at the bottom. The value obtained from Eq. 20 is also shown for comparison (triangles).

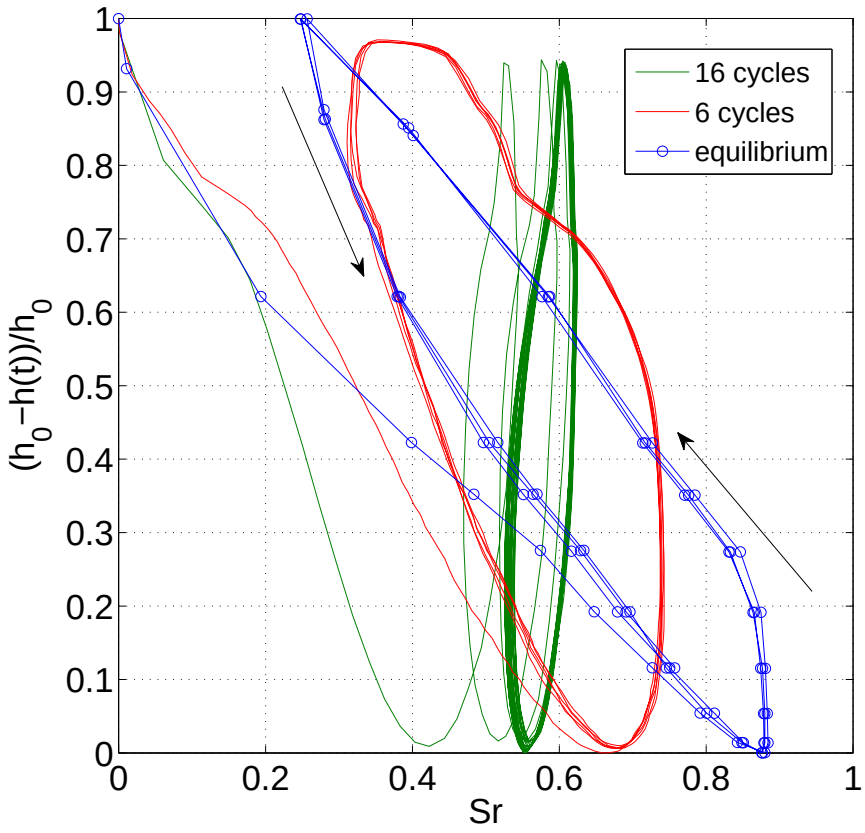

Figure 8: Imposed hydraulic head fluctuations $(h_0 - h(t))/h_0$ versus the saturation variations (Sr) for two different frequencies and 4 cycles of equilibrium simulations. The arrows shows the time sequence taking for the equilibrium cycles, first imbibition and then drainage, which also holds for the dynamic simulations.

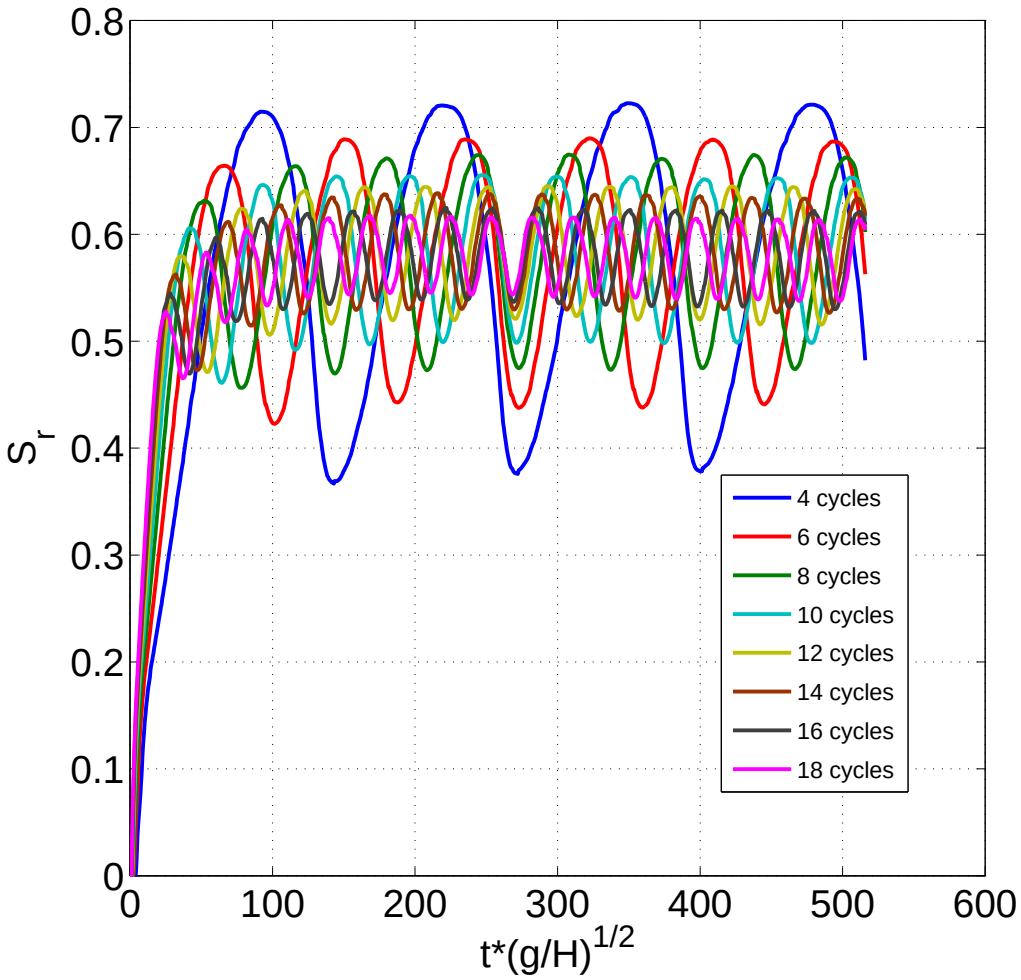

Figure 9: Water saturation Sr as a function of dimensionless time (time multiplied by the factor $\sqrt{g/H}$) from simulations with different frequencies (as indicated by the number of fluctuation cycles within the period of the plots).

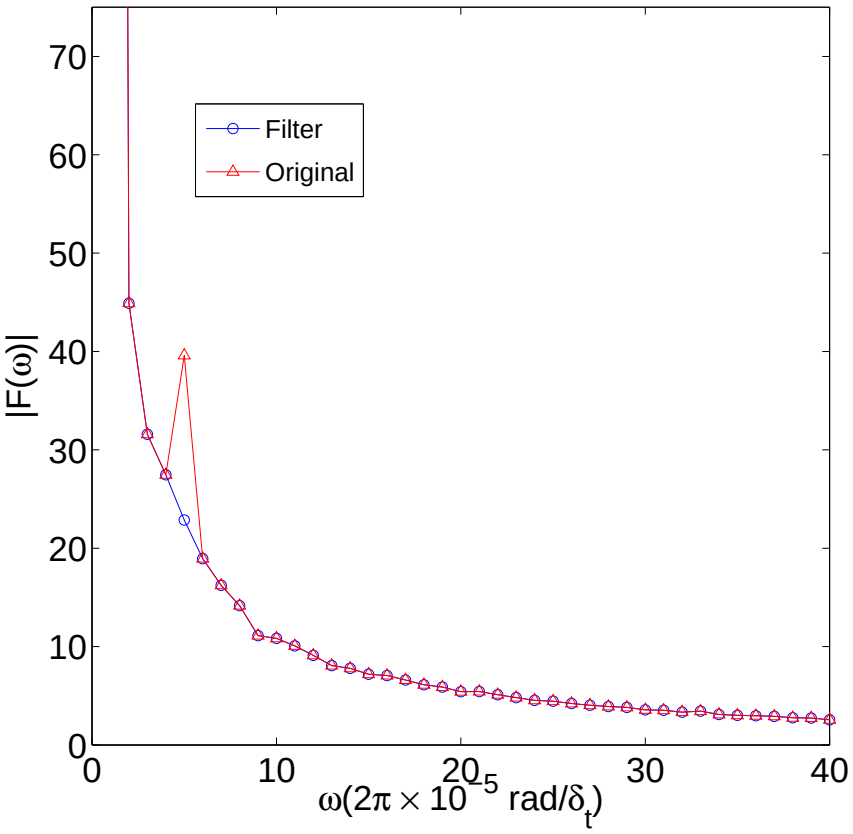

Figure 10: Amplitude of the Fourier components $|F(\omega)|$ for each frequency for both original (triangles) and filtered signals (squares).

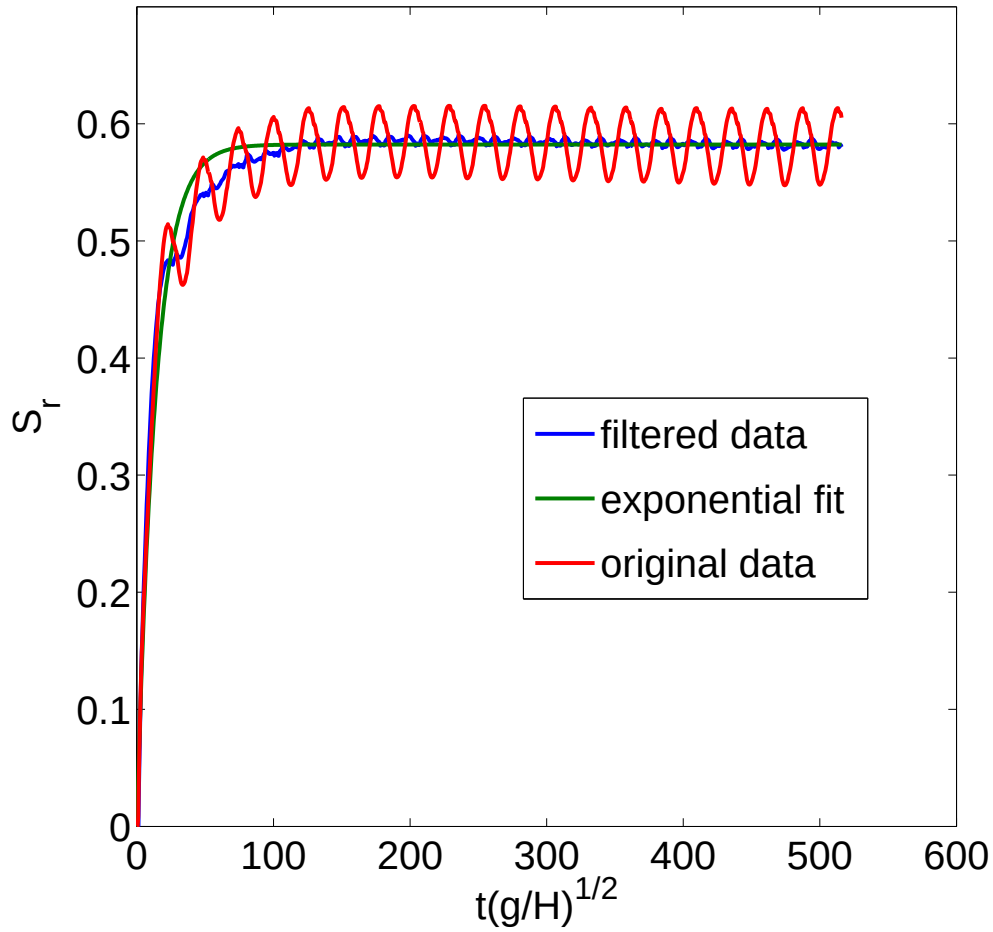

Figure 11: Function $Sr(t)$ after the filtering process (blue) fitted with the exponential component of Eq. 22 (green) and the original data (red).

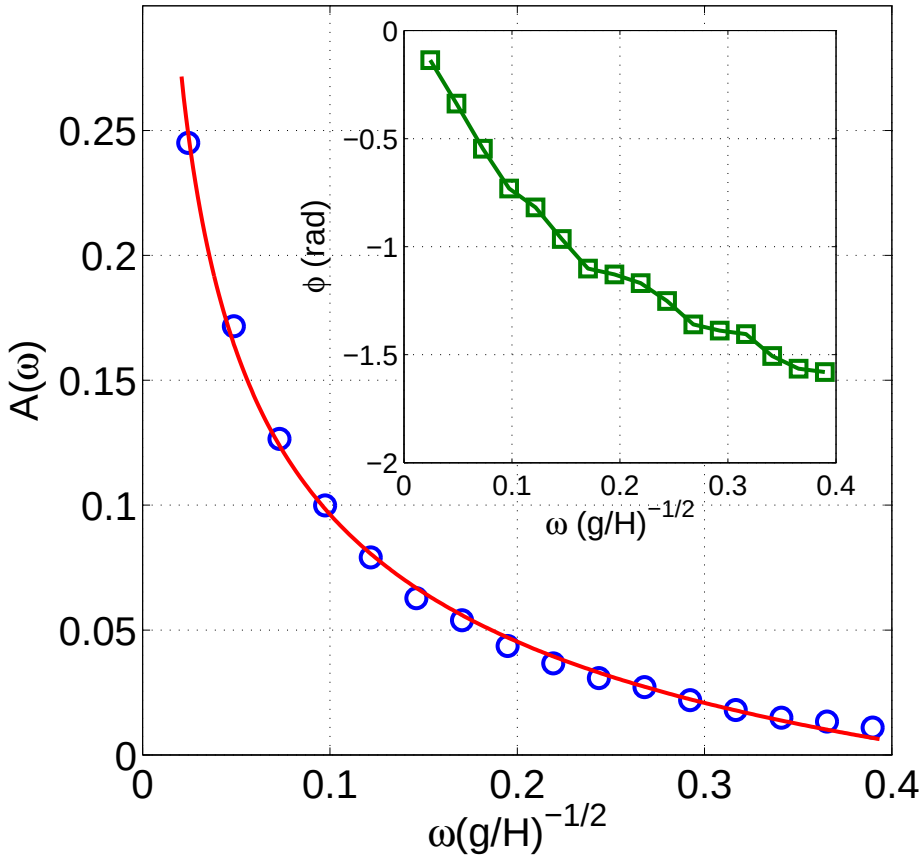

Figure 12: Amplitude $A(\omega)$ of the harmonic component of $Sr(t)$ as a function of ω with a power law fitting (exponent equal to -0.36). Inset: phase angle ϕ representing the lag of the Sr oscillation behind the imposed head fluctuation.

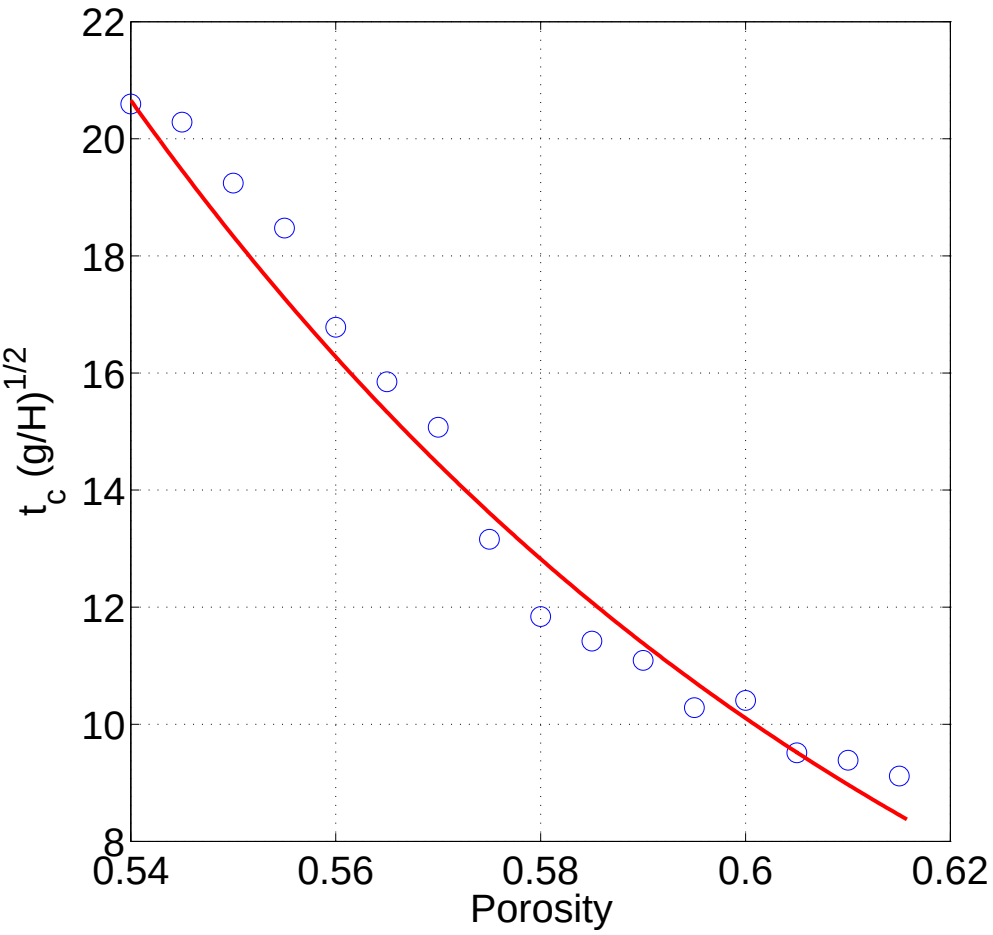

Figure 13: Characteristic time t_c versus porosity. The red line is provided as a visual aid, not based on any particular fitting function.